Dynamics of the Space Tug System with a Short Tether

Liu, J., Cui, N., Shen, F., & Rong, S. (2015). Dynamics of the Space Tug System with a Short Tether. International Journal of Aerospace Engineering, 2015, [740253]. https://doi.org/10.1155/2015/740253

Published in:
International Journal of Aerospace Engineering

Document Version:
Publisher's PDF, also known as Version of record

Hindawi Publishing Corporation
International Journal of Aerospace Engineering
Volume 2015, Article ID 740253, 16 pages
http://dx.doi.org/10.1155/2015/740253

Research Article

Dynamics of the Space Tug System with a Short Tether

Jiafu Liu,[1] Naigang Cui,[2] Fan Shen,[2] and Siyuan Rong[2]

[1]*Shenyang Aerospace University, Shenyang 110136, China*
[2]*Harbin Institute of Technology, Harbin 150001, China*

Correspondence should be addressed to Jiafu Liu; liujiafuericking@163.com

Received 25 February 2015; Revised 12 June 2015; Accepted 2 July 2015

Academic Editor: Paul Williams

The dynamics of the space tug system with a short tether similar to the ROGER system during deorbiting is presented. The kinematical characteristic of this system is significantly different from the traditional tethered system as the tether is tensional and tensionless alternately during the deorbiting process. The dynamics obtained based on the methods for the traditional tethered system is not suitable for the space tug system. Therefore, a novel method for deriving dynamics for the deorbiting system similar to the ROGER system is proposed by adopting the orbital coordinates of the two spacecraft and the Euler angles of ROGER spacecraft as the generalized coordinates instead of in- and out-plane librations and the length of the tether and so forth. Then, the librations of the system are equivalently obtained using the orbital positions of the two spacecraft. At last, the geostationary orbit (GEO) and the orbit whose apogee is 300 km above GEO are chosen as the initial and target orbits, respectively, to perform the numerical simulations. The simulation results indicate that the dynamics can describe the characteristic of the tether-net system conveniently and accurately, and the deorbiting results are deeply affected by the initial conditions and parameters.

1. Introduction

The number of flying objects including the controlled spacecraft and the space debris (including the abandoned spacecraft) in the low earth orbit (LEO) and the geostationary orbit (GEO) increases sharply because of the frequent human space activities [1–3]. It is reported by ESA that, at the end of 2008, there were 1186 objects in GEO and only 32% were controlled spacecraft. The collision risks will be posed by the uncontrolled spacecraft and space debris mentioned above. Therefore, it is necessary to monitor and clear the abandoned spacecraft and space debris.

The RObotic GEostationary Orbit Restorer (ROGER) concept was proposed by ESA. The researchers not only focused on the economic consideration and future business application but also focused on the orbital monitoring and clearance of the abandoned spacecraft [4, 5]. To make use of the space electrodynamic tethered system to deorbit spacecraft has been studied in [6, 7], which utilizes the motion of the conductive tether relative to the magnetic field of the earth to produce electrodynamic forces. It is also proposed that the abandoned spacecraft can be deorbited by the solar radiation pressure experienced by the sailcraft attached to the spacecraft. The sailcraft is initially folded and will be deployed when the spacecraft is spent. The feasibility of the solar radiation pressure based deorbiting approach has been demonstrated by the NanoSail-D project within NASA. Moreover, the cubeSail project in Surrey [8] and the project using solar pressure in Strathclyde [9] are also performed to study the spacecraft deorbiting approach by solar pressure. It is a practical method by using the space robots to capture the noncooperative spacecraft or to deorbit the abandoned spacecraft. The method can also be used in the space missions such as spacecraft repair and fuel charges [10, 11].

The space tether based deorbiting system is the most comprehensively studied one among the methods mentioned above, including the ROGER system and the space electrodynamic tethered system.

The monitoring for the current orbit and forecasting for the future orbit are studied in the ROGER project [5]. The feasibility of the GEO service is also discussed from the view of economic and technical aspects. The ROGER spacecraft approaches, captures, and transports the abandoned spacecraft into the graveyard orbit. The configuration of the

ROGER system including the ROGER spacecraft and the subsystem used for capturing the abandoned spacecraft is studied and developed in ESA. The technical details of the ROGER system mainly focus on the grappling equipment, attitude and orbit control devices and so forth. Moreover, the guidance, navigation, and control elements are also focused on [4].

The typical electrodynamic tethered system for deorbiting is MXER, which utilizes the electrodynamic force to deorbit the spacecraft. The system design is presented in [12, 13]. The studies concerning space tethered system mainly focus on tether models [14, 15], tether vibrations [16–19], in-plane and out-plane librations [20–26], attitude motions [19, 27–30], and orbital motions [31–33]. The bead model is adopted to establish the dynamical equations in [14, 15]. Input Shaping method is adopted to reduce the initial vibrations of the electrodynamic tether system in [34]. The stability of in-plane and out-plane librations of the electrodynamic tethered system in inclined and elliptic orbits with high eccentricity is studied in [25, 26], and the chaotic librations can be stabilized to the periodic motion by delayed feedback control. The attitude control of the main satellite can be performed by the offset scheme [27]. The vibration of the tether can also be suppressed by the offset scheme [19]. There are a large number of literatures concerning with space tethered system, however, few concerning with the system design and dynamics for the space tug system similar to the ROGER system during deorbiting. It seems that the configurations of the tethered systems in [35, 36] are analogous to the ROGER system; however, there exist differences between them.

The paper is organized as follows. Firstly, the configuration that the ROGER spacecraft in front of the abandoned one is adopted, the reference frames and coordinate transformations are presented. Secondly, the conclusion that the traditional dynamic modeling strategy for the tethered system is not suitable for the space tug system similar to the ROGER system in this paper is presented. Thirdly, the dynamic model for the space short-tether system during deorbiting is presented. The attitude motion of the ROGER spacecraft, the orbital motion of the two spacecraft, the librations of the system, and the elasticity of the tether are all considered. Finally, the effectiveness of the dynamic model is verified by numerical simulations. The superior deorbiting conditions are summarized based on the simulation results for various parameters and initial conditions.

2. The Roger System and Reference Frames

2.1. The Configuration, Simplification, and Assumption. The configuration of the space tug system with a short tether similar to the ROGER system is presented in Figure 1. As shown in Figure 1, the active (the ROGER) spacecraft and the abandoned spacecraft are denoted as "A" and "B," respectively.

The tether is tensional and tensionless alternatively during the deorbiting process because the ROGER spacecraft is in front of (not above) the abandoned one.

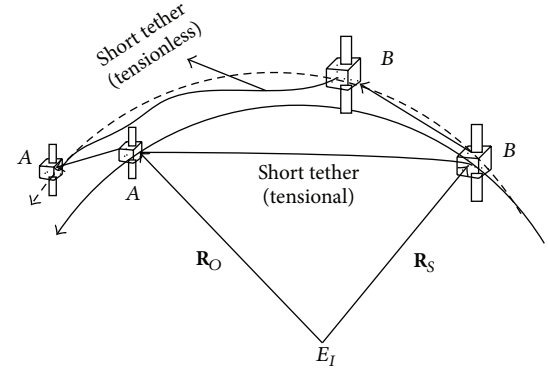

Figure 1: The schematic diagram of the space tug system with a short tether similar to the ROGER system during deorbiting.

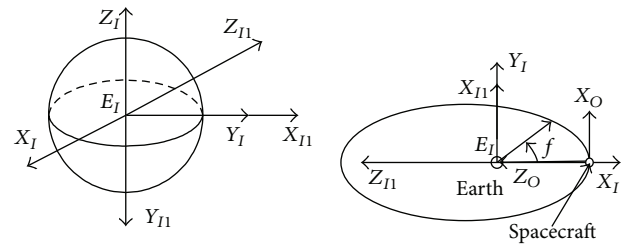

Figure 2: The related reference frames.

Some assumptions are presented as follows:

(1) The attitude motion of the abandoned spacecraft is neglected and only the orbital motion is considered.

(2) The mass of the short tether is neglected.

(3) Solar radiation pressure perturbation, earth nonspherical perturbation, and other planets perturbation are neglected.

2.2. Reference Frames and Transformations

2.2.1. Inertial Frame J2000 ($\mathbf{E}_I\mathbf{X}_I\mathbf{Y}_I\mathbf{Z}_I, \pi_I$). E_I is the mass center of the earth, $\mathbf{E}_I\mathbf{X}_I$ points to the vernal equinox, $\mathbf{E}_I\mathbf{Y}_I$ points to the earth's rotation axis perpendicular to the equatorial plane, and $\mathbf{E}_I\mathbf{X}_I$, $\mathbf{E}_I\mathbf{Y}_I$, and $\mathbf{E}_I\mathbf{Z}_I$ form a right-handed orthogonal frame. The basis of π_I is $(\mathbf{i}_I, \mathbf{j}_I, \mathbf{k}_I)^T$.

2.2.2. The ROGER Spacecraft Orbital ($\mathbf{O}_O\mathbf{X}_O\mathbf{Y}_O\mathbf{Z}_O, \pi_O$) and Body ($\mathbf{O}_O\mathbf{X}_A\mathbf{Y}_A\mathbf{Z}_A, \pi_A$) Frames. O_O locates at the mass center of "A," $\mathbf{O}_O\mathbf{Z}_O$ points to E_I, and $\mathbf{O}_O\mathbf{X}_O$ points to forward direction located in the orbital plane and perpendicular to $\mathbf{O}_O\mathbf{Z}_O$. $\mathbf{O}_O\mathbf{X}_O$, $\mathbf{O}_O\mathbf{Y}_O$, and $\mathbf{O}_O\mathbf{Z}_O$ form a right-handed orthogonal frame. The basis is $(\mathbf{i}_O, \mathbf{j}_O, \mathbf{k}_O)^T$.

The origin of π_A is at the mass center of "A," with the axes pointing along the principal axes of inertia of "A." The basis is $(\mathbf{i}_A, \mathbf{j}_A, \mathbf{k}_A)^T$.

2.2.3. Inertial Frame ($\mathbf{E}_I\mathbf{X}_{I1}\mathbf{Y}_{I1}\mathbf{Z}_{I1}, \pi_{I1}$). The detailed definition can be found in Figure 2. The basis is $(\mathbf{i}_{I1}, \mathbf{j}_{I1}, \mathbf{k}_{I1})^T$.

2.2.4. Body Frame of the Tether ($\mathbf{C}_A\mathbf{X}_t\mathbf{Y}_t\mathbf{Z}_t, \pi_t$). C_A is the attachment point with "A," when there are no librations, and π_t coincides with π_O. The in-plane and out-plane librations in traditional tethered system are defined by the angles between π_O and π_t.

2.2.5. The Transformation from π_A to π_O. A three-element vector $(\psi_A, \varphi_A, \theta_A)^T$ is used to describe the attitude of the ROGER spacecraft with respect to the orbital frame. The transformation from π_O to π_A can be realized by 3-1-2, that is, $z(\psi_A) \rightarrow x(\varphi_A) \rightarrow y(\theta_A)$ rotation. $\psi_A, \varphi_A, \theta_A$ are the Euler angles of yaw-roll-pitch describing attitude motion for the ROGER spacecraft.

2.2.6. The Transformation from π_{I1} to π_O. The rotation matrix $\mathbf{C}_{OI1}$ is obtained by a $y(-f - f_1)$ rotation, and the initial true anomaly f_1 is selected as zero. f is the true anomaly. $\mathbf{C}_{OI1}$ is as follows:

$$\mathbf{C}_{OI1} = \begin{bmatrix} \cos(-f) & 0 & -\sin(-f) \\ 0 & 1 & 0 \\ \sin(-f) & 0 & \cos(-f) \end{bmatrix}. \tag{1}$$

2.2.7. The Transformation from π_O to π_t. A two-element vector $(\psi, \theta)^T$ is used to describe the attitude of the tether with respect to the orbital frame. The transformation from $\mathbf{O}_O\mathbf{X}_O\mathbf{Y}_O\mathbf{Z}_O$ to $\mathbf{C}_A\mathbf{X}_t\mathbf{Y}_t\mathbf{Z}_t$, can be realized by a $z(\psi) \rightarrow y(\theta)$ rotation. The rotation matrix $\mathbf{C}_{tO}$ is as follows:

$$\mathbf{C}_{tO} = \begin{bmatrix} \cos\theta & 0 & -\sin\theta \\ 0 & 1 & 0 \\ \sin\theta & 0 & \cos\theta \end{bmatrix} \begin{bmatrix} \cos\psi & \sin\psi & 0 \\ -\sin\psi & \cos\psi & 0 \\ 0 & 0 & 1 \end{bmatrix}. \tag{2}$$

2.2.8. The Transformation from π_I to π_O. The constant rotation matrix $\mathbf{C}_{I1I}$ is obtained by a 3-1 rotation, presented as follows:

$$\mathbf{C}_{I1I} = \begin{bmatrix} 1 & 0 & 0 \\ 0 & \cos(-90^\circ) & \sin(-90^\circ) \\ 0 & -\sin(-90^\circ) & \cos(-90^\circ) \end{bmatrix} \begin{bmatrix} \cos 90^\circ & \sin 90^\circ & 0 \\ -\sin 90^\circ & \cos 90^\circ & 0 \\ 0 & 0 & 1 \end{bmatrix}. \tag{3}$$

Thus, the transformation from π_I to π_O is obtained as $\mathbf{C}_{OI} = \mathbf{C}_{OI1}\mathbf{C}_{I1I}$.

3. The Traditional Dynamic Modeling Method for the Roger System

3.1. The Selection of the Generalized Coordinates. In order to study the dynamics of the ROGER system during deorbiting, the attitude and orbital motions of the ROGER spacecraft, in-plane and out-plane librations of the system, the length motion of the tether, and orbital motion of the abandoned spacecraft are studied in this paper. When the tether is tensional, the Euler angles ψ_A, φ_A, and θ_A and orbital positions x_A, y_A, and z_A are chosen as the generalized coordinates; moreover, the length of the tether l and the in-plane and out-plane librations ψ, θ are also chosen as the generalized coordinates. When the tether is tensionless, the strategy to choose the generalized coordinates will be discussed later.

3.2. Dynamic Modeling Consideration When the Tether Is Tensional. The Lagrange method is used to establish the dynamics for the ROGER system. The kinetic energy T_A and gravitational potential energy U_A of the ROGER spacecraft are as follows:

$$\begin{aligned} T_A &= \frac{1}{2}\int_A (\dot{\mathbf{r}}_A + \boldsymbol{\omega}_A \times \mathbf{r}) \cdot (\dot{\mathbf{r}}_A + \boldsymbol{\omega}_A \times \mathbf{r})\, dm \\ &= \frac{1}{2} m_A |\dot{\mathbf{r}}_A|^2 + \frac{1}{2}\boldsymbol{\omega}_A \cdot \mathbb{J}_A \cdot \boldsymbol{\omega}_A \\ U_A &= -\frac{\mu m_A}{|\mathbf{r}_A|}, \end{aligned} \tag{4}$$

where $\mathbf{r}_A$ and $\dot{\mathbf{r}}_A$ are the position and velocity vectors of point A, $\boldsymbol{\omega}_A$ is the angular velocity of the ROGER spacecraft, and $\mathbf{r}$ and $\mathbf{r}_m$ are the position vectors of the infinitesimal mass dm with respect to point A and E_I, respectively. m_A is the mass. $\mathbb{J}_A$ is the moment of inertia tensor. μ is Earth's gravitational constant. $\mathbf{r}_{C_A}$ (constant in π_A) is the position vector of the attachment point with respect to point A. $\mathbf{r}_{C_AB}$ is the position vector of the abandoned spacecraft with respect to C_A. In this paper, $|\mathbf{r_{AB}}|$ is adopted as the length of the tether instead of $|\mathbf{r}_{C_AB}|$. The kinetic energy T_B and gravitational potential energy U_B are as follows:

$$\begin{aligned} T_B &= \frac{1}{2} m_B \left[\dot{\mathbf{r}}_A + \mathring{\mathbf{l}}\,(t) + \boldsymbol{\omega}_t \times \mathbf{l}(t)\right] \\ &\quad \cdot \left[\dot{\mathbf{r}}_A + \mathring{\mathbf{l}}\,(t) + \boldsymbol{\omega}_t \times \mathbf{l}(t)\right], \\ U_B &= -\frac{\mu m_B}{|\mathbf{r}_A + \mathbf{l}(t)|}. \end{aligned} \tag{5}$$

The elastic potential energy of the tether is as follows:

$$U_e = \frac{1}{2} k (l - l_0)^2. \tag{6}$$

In the preceding three equations, m_B and $\dot{\mathbf{r}}_B$ indicate the mass and velocity of the abandoned spacecraft. $\dot{\mathbf{l}}(t)$ and $\mathring{\mathbf{l}}\,(t)$ are the derivatives of $\mathbf{l}(t)$ relative to π_I and π_t, respectively. $\boldsymbol{\omega}_t$ is the angular velocity of the tether. k is the coefficient of elasticity of the tether. l_0 is the original length of the tether.

The Lagrange equation considering nonpotential force is as follows:

$$\frac{d}{dt}\left(\frac{\partial L}{\partial \dot{\mathbf{q}}_j}\right) - \frac{\partial L}{\partial \mathbf{q}_j} = \mathbf{Q}_j, \tag{7}$$

where $\mathbf{Q}_j$ is the nonpotential force containing the thrust force and the attitude control torques generated by the ROGER spacecraft. $\mathbf{q}_j = (x_A, y_A, z_A, \psi_A, \varphi_A, \theta_A, \psi, \theta, l)^T$ is the vector of the generalized coordinates. The dynamic modeling procedure above can be used when the tether is tensional.

3.3. Dynamic Modeling Consideration When the Tether Is Tensionless. The ROGER and abandoned spacecraft become two free flying spacecraft orbiting the earth when the tether is tensionless. Thus, the orbital position coordinates (x_A, y_A, z_A) and (x_B, y_B, z_B) of the ROGER and abandoned spacecraft, and the Euler angles $(\psi_A, \varphi_A, \theta_A)$ of the ROGER spacecraft are selected as the generalized coordinates when the tether is tensionless.

3.4. Analysis of the Traditional Method. The dynamic modeling method presented above is just the dynamic modeling strategy for the traditional tethered system. To select the in-plane and out-plane librations and the length of the tether as the generalized coordinates is inappropriate for establishing the dynamics of the ROGER system in this paper, although it is easy to be understood. The reasons are presented as follows:

(1) The ROGER spacecraft is in front of (not above) the abandoned spacecraft during deorbiting; therefore the tether will be tensional and tensionless alternately. The in-plane and out-plane librations and the length of the tether can be selected as the generalized coordinates when the tether is tensional; however, the librations and the length of the tether never exist when the tether is tensionless.

(2) It is assumed that the tether is tensional initially as shown in Figure 3. It is evident that the tether will become tensionless when $l = 30$ and $\dot{l} < 0$. The dynamic model when the tether is tensionless will be used. And the tether will become tensional when $l = 30$ and $\dot{l} > 0$. Accordingly, the dynamic model when the tether is tensional will be used.

The critical points are presented in Figure 4. It is evident that the tether will be tensionless at points 1, 3, and 5 and tensional at points 2, 4, and 6.

(3) It is time-consuming and difficult to switch repeatedly between the two groups of equations that can be derived based on the ideas stated in Sections 3.2 and 3.3; moreover, the computation accuracy and real-time requirements cannot be satisfied during deorbiting. Therefore, it is essential to establish a unique group of dynamic equation for the deorbiting process using a unique group of generalized coordinates.

Therefore, the ROGER and abandoned spacecraft orbital position coordinates (x_A, y_A, z_A) and (x_B, y_B, z_B) and the Euler angles $(\psi_A, \varphi_A, \theta_A)$ of the ROGER spacecraft are adopted as the generalized coordinates rather than the librations and the length of the tether.

4. The Dynamics of the Tether System

The orbital position coordinates of the ROGER and abandoned spacecraft and the Euler angles of ROGER spacecraft are adopted as the generalized coordinates instead of the librations and the length of the tether because the following relation holds:

$$(\psi, \theta, l, x_A, y_A, z_A) \Longleftrightarrow (x_B, y_B, z_B, x_A, y_A, z_A). \quad (8)$$

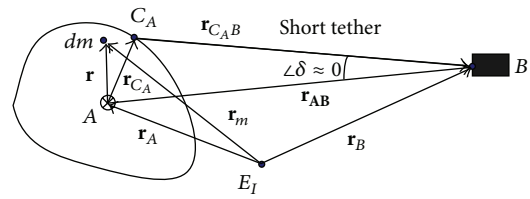

Figure 3: The detailed configuration of the ROGER spacecraft.

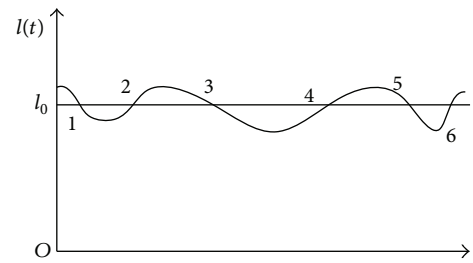

Figure 4: The length of the tether with the critical points (1–6).

The kinetic energy of the ROGER system is as follows:

$$\begin{aligned} T &= T_A + T_B, \\ T_A &= \frac{1}{2} m_A \left(\dot{x}_A^2 + \dot{y}_A^2 + \dot{z}_A^2\right) + \frac{1}{2} \boldsymbol{\omega}_A \cdot \mathbb{J}_A \cdot \boldsymbol{\omega}_A, \\ T_B &= \frac{1}{2} m_B \left(\dot{x}_B^2 + \dot{y}_B^2 + \dot{z}_B^2\right). \end{aligned} \quad (9)$$

The potential energy is as follows:

$$\begin{aligned} U &= U_g + U_e, \\ U_g &= U_{gA} + U_{gB}, \\ U_{gA} &= -\frac{\mu m_A}{\sqrt{x_A^2 + y_A^2 + z_A^2}}, \\ U_{gB} &= -\frac{\mu m_B}{\sqrt{x_B^2 + y_B^2 + z_B^2}}. \end{aligned} \quad (10)$$

The elastic potential energy of the tether is as follows by referring to Figure 3:

$$\begin{aligned} U_e &= \begin{cases} 0 & \left|\mathbf{r}_{C_AB}\right| \le l_0 \\ \frac{1}{2} k \Delta^2 & \left|\mathbf{r}_{C_AB}\right| > l_0 \end{cases} \\ \Delta &= \left|\mathbf{r}_{C_AB}\right| - l_0, \\ l &= \mathbf{r}_{C_AB} = \mathbf{r}_B - \mathbf{r}_A - \mathbf{r}_{C_A}. \end{aligned} \quad (11)$$

The related position vectors in the preceding equation can be observed in Figure 3. All the position vectors are easy to obtain since $\mathbf{r}_{C_A}$ is constant in π_A.

The Lagrange function of the ROGER system is as follows:

$$\begin{aligned} L &= T - U = T_A + T_B - U_{gA} - U_{gB} - U_e \\ &= \frac{1}{2} m_A \left(\dot{x}_A^2 + \dot{y}_A^2 + \dot{z}_A^2 \right) + \frac{1}{2} \boldsymbol{\omega}_A \cdot \mathbb{J}_A \cdot \boldsymbol{\omega}_A \\ &\quad + \frac{1}{2} m_B \left(\dot{x}_B^2 + \dot{y}_B^2 + \dot{z}_B^2 \right) - \left(-\frac{\mu m_A}{\sqrt{x_A^2 + y_A^2 + z_A^2}} \right) \\ &\quad - \left(-\frac{\mu m_B}{\sqrt{x_B^2 + y_B^2 + z_B^2}} \right) - U_e. \end{aligned} \tag{12}$$

The dynamic equations will be obtained when L is substituted into the Lagrange equations.

4.1. Dynamic Equations for Tensional State. Firstly, the orbital motion of the ROGER spacecraft is given as follows:

$$\begin{aligned} \ddot{x}_A &= -\frac{\mu x_A}{\left(x_A^2 + y_A^2 + z_A^2\right)^{3/2}} + \frac{k\Delta \left(x_B - x_A - r_x\right)}{m_A \left|\mathbf{r}_{C_A B}\right|} + F_x, \\ \ddot{y}_A &= -\frac{\mu y_A}{\left(x_A^2 + y_A^2 + z_A^2\right)^{3/2}} + \frac{k\Delta \left(y_B - y_A - r_y\right)}{m_A \left|\mathbf{r}_{C_A B}\right|} + F_y, \\ \ddot{z}_A &= -\frac{\mu z_A}{\left(x_A^2 + y_A^2 + z_A^2\right)^{3/2}} + \frac{k\Delta \left(z_B - z_A - r_z\right)}{m_A \left|\mathbf{r}_{C_A B}\right|} + F_z, \end{aligned} \tag{13}$$

where r_x, r_y, and r_z are the components of $\mathbf{r}_{C_A}$ in π_I.

Secondly, the attitude motion equation of the ROGER spacecraft is as follows:

$$\mathbb{J}_A \cdot \dot{\boldsymbol{\omega}}_A + \boldsymbol{\omega}_A \times \mathbb{J}_A \cdot \boldsymbol{\omega}_A = \mathbf{T}_c + \mathbf{T}_d, \tag{14}$$

where $\mathbf{T}_c$ is the control torque and $\mathbf{T}_d$ is the disturbance torque caused by the offset of the thrust force, the librations of the tether combining the tension of the tether. $\mathbf{T}_{df}$ and $\mathbf{T}_{dt}$ are used to represent the former and the latter disturbance torques, respectively.

As shown in Figure 5, the offset vector **AP**, the components of the thrust force, and $\mathbf{T}_{dt}$ are as follows:

$$\begin{aligned} \mathbf{AP} &= \mathbf{r}_p = r_{py}\mathbf{j}_A + r_{pz}\mathbf{k}_A, \\ \mathbf{F} &= F_x \mathbf{i}_A, \\ \mathbf{T}_{dt} &= \mathbf{r}_p \times \mathbf{F}. \end{aligned} \tag{15}$$

We can obtain $\mathbf{T}_{df}$ as $\mathbf{T}_{df} = \mathbf{r}_{C_A} \times \mathbf{T}$. $\mathbf{r}_{C_A}$ and $\mathbf{T}$ can be calculated during deorbiting.

The procedure to obtain the orbital motion of the abandoned spacecraft is similar to the ROGER spacecraft.

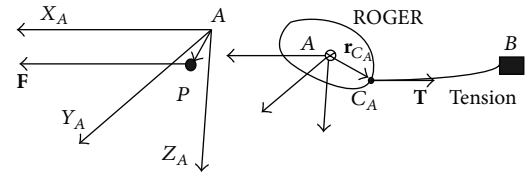

Figure 5: The disturbance torques.

4.2. The Dynamic Equations regardless of the State (Tensional or Tensionless) of the Tether. The orbital and attitude dynamic equations of the ROGER spacecraft are as follows:

$$\begin{aligned} &\ddot{x}_A \\ &= -\frac{\mu x_A}{\left(x_A^2 + y_A^2 + z_A^2\right)^{3/2}} + F_x \\ &\quad + \begin{cases} \dfrac{k\Delta \left(x_B - x_A - r_x\right)}{m_A \left|\mathbf{r}_{C_A B}\right|} & (l \geq l_0) \\ 0 & (l < l_0), \end{cases} \\ &\ddot{y}_A \\ &= -\frac{\mu y_A}{\left(x_A^2 + y_A^2 + z_A^2\right)^{3/2}} + F_y \\ &\quad + \begin{cases} \dfrac{k\Delta \left(y_B - y_A - r_y\right)}{m_A \left|\mathbf{r}_{C_A B}\right|} & (l \geq l_0) \\ 0 & (l < l_0), \end{cases} \\ &\ddot{z}_A \\ &= -\frac{\mu z_A}{\left(x_A^2 + y_A^2 + z_A^2\right)^{3/2}} + F_z \\ &\quad + \begin{cases} \dfrac{k\Delta \left(z_B - z_A - r_z\right)}{m_A \left|\mathbf{r}_{C_A B}\right|} & (l \geq l_0) \\ 0 & (l < l_0) \end{cases} \\ &\mathbb{J} \cdot \dot{\boldsymbol{\omega}} + \boldsymbol{\omega} \times \mathbb{J} \cdot \boldsymbol{\omega} = \begin{cases} \mathbf{T}_c + \mathbf{T}_{df} + \mathbf{T}_{dt} & (l \geq l_0) \\ \mathbf{T}_c + \mathbf{T}_{df} & (l < l_0). \end{cases} \end{aligned} \tag{16}$$

The Gaussian perturbation equations are used to perform the dynamics simulations:

$$\begin{aligned} \frac{da}{dt} &= \frac{2}{n\sqrt{1-e^2}} \left(\sigma_z e \sin f + \sigma_x \frac{p}{r} \right), \\ \frac{d\Omega}{dt} &= \frac{\sigma_y r \sin u}{na^2 \sqrt{1-e^2} \sin i}, \\ \frac{di}{dt} &= \frac{\sigma_y r \cos u}{na^2 \sqrt{1-e^2}}, \end{aligned}$$

$$\frac{de_x}{dt} = \frac{\sqrt{1-e^2}}{na}\left\{\sigma_z \sin u + \sigma_x\left[\left(1+\frac{r}{p}\right)\cos u + \frac{r}{p}e_x\right]\right\} + \frac{d\Omega}{dt}e_y \cos i,$$

$$\frac{de_y}{dt} = \frac{\sqrt{1-e^2}}{na}\left\{-\sigma_z \cos u + \sigma_x\left[\left(1+\frac{r}{p}\right)\sin u + \frac{r}{p}e_y\right]\right\} - \frac{d\Omega}{dt}e_x \cos i,$$

$$\frac{d\varphi}{dt} = n - \frac{1}{na}\left[\sigma_z\left(\frac{2r}{a} + \frac{\sqrt{1-e^2}}{1+\sqrt{1-e^2}}e\cos f\right) - \sigma_x\left(1+\frac{r}{p}\right)\frac{\sqrt{1-e^2}}{1+\sqrt{1-e^2}}e\sin f\right] - \frac{\sigma_y r \cos i \sin u}{na^2\sqrt{1-e^2}\sin i}, \tag{17}$$

where $(a, \Omega, i, e_x, e_y, \varphi)$ are six independent orbital elements for the ROGER and abandoned spacecraft. In the paper, a, Ω, and i denote the semimajor axis, longitude of ascending node of the orbit, and orbital inclination. Please note that $e_x = e\cos\omega$, $e_y = e\sin\omega$ and φ (sum of mean anomaly and argument of perigee) are used instead of the orbital eccentricity e, argument of perigee ω, and true anomaly ν to avoid singularity when e approaches zero. n, p, r, and u are the mean orbital rate, semilatus rectum of an orbit, geocentric radius, and sum of true anomaly and argument of perigee, respectively. σ_x, σ_y, and σ_z are the components of the perturbative accelerations along x-, y-, and z-axis of π_O.

4.3. Equivalent Expression of Librations. It is evident that the ROGER system will never librate when the tether is tensionless and tensional alternately during deorbiting, which is quite different from the traditional space tethered system. A novel strategy to equivalently express the librations of the ROGER system has been proposed based on the positions of the ROGER and abandoned spacecraft.

As in Figure 6(a), the direction cosines of line section **AB** in $\mathbf{E}_I\mathbf{X}_I\mathbf{Y}_I\mathbf{Z}_I$ are expressed as follows:

$$\lambda_1 = \cos(\mathbf{AB}, \mathbf{i}_I) = \frac{(x_A - x_B)}{|\mathbf{AB}|},$$
$$\lambda_2 = \cos(\mathbf{AB}, \mathbf{j}_I) = \frac{(y_A - y_B)}{|\mathbf{AB}|}, \tag{18}$$
$$\lambda_3 = \cos(\mathbf{AB}, \mathbf{k}_I) = \frac{(z_A - z_B)}{|\mathbf{AB}|}.$$

The direction cosines in $\mathbf{O}_O\mathbf{X}_O\mathbf{Y}_O\mathbf{Z}_O$ are expressed as follows:

$$\begin{bmatrix}\gamma_x \\ \gamma_y \\ \gamma_z\end{bmatrix}_O = \mathbf{C}_{OI}\begin{bmatrix}\lambda_1 \\ \lambda_2 \\ \lambda_3\end{bmatrix}_I, \tag{19}$$

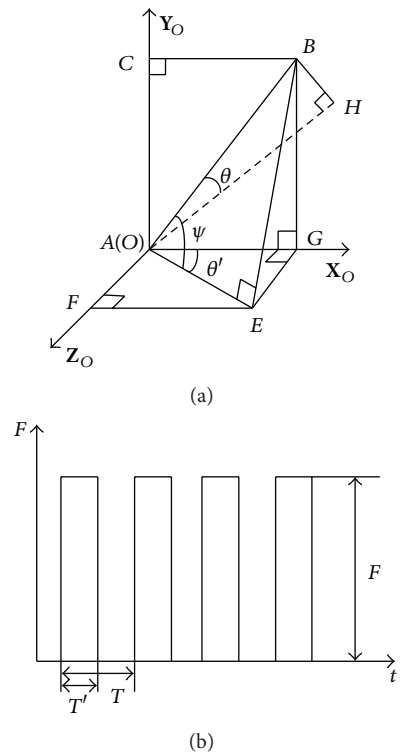

Figure 6: The librations (a) and the thrust force (b).

where γ_x, γ_y, and γ_z are the components of the direction cosines in $\mathbf{O}_O\mathbf{X}_O\mathbf{Y}_O\mathbf{Z}_O$. The out-plane ($\psi$) and in-plane ($\theta$) librations can be obtained later. And the coordinate transformation matrix $\mathbf{C}_{OI}$ has been derived before.

As shown in Figure 6, line sections BH and BE are perpendicular to planes $A\mathbf{X}_O\mathbf{Z}_O$ and $A\mathbf{X}_O\mathbf{Y}_O$, respectively. And the in-plane and out-plane librations can be expressed as follows:

$$\psi = \arcsin\left(\frac{BE}{|\mathbf{AB}|}\right) = \gamma_y,$$
$$\theta = \arcsin\left(\frac{BH}{|\mathbf{AB}|}\right) = \gamma_z. \tag{20}$$

The definition above will be better than the traditional one as there is no singularity.

4.4. Nonpotential Force of the ROGER Spacecraft. The purpose of this paper is to transport the abandoned spacecraft into the orbit whose apogee is 300 km above GEO. The thrust force direction is $\mathbf{n} = -\mathbf{r} \times (\mathbf{r} \times \mathbf{v})/|\mathbf{r} \times (\mathbf{r} \times \mathbf{v})|$, where $\mathbf{n}$, $\mathbf{r}$, and $\mathbf{v}$ are the unit vectors of the thrust force, the position, and velocity of the ROGER spacecraft, respectively. The amplitude, period, and duty cycle of the thrust force can be obtained by referring to Figure 6. F and $\eta = T'/T$ are the amplitude and duty cycle of the thrust force. The vector of the thrust force can be written as $\mathbf{F} = F_x\mathbf{i}_A + F_y\mathbf{j}_A + F_z\mathbf{k}_A$.

The components of $\mathbf{T}_C$ in $\mathbf{O}_O\mathbf{X}_A\mathbf{Y}_A\mathbf{Z}_A$ can be written as $\mathbf{T}_C = T_x\mathbf{i}_A + T_y\mathbf{j}_A + T_z\mathbf{k}_A$.

Table 1: The cases with different parameters.

	Rm0	**Rs**0	k	T	η
Case 1	$[42114203 - 0.3, 0, -0.2]^T$	$[42114203 + 1.2, -29.2, 1.5]^T$	5000	0.5	50%
Case 2	$[42114203, 0, 0]^T$	$[42114203, -29.28788, 0]^T$	5000	0.5	50%
Case 3	$[42114203 - 0.3, 0, -0.2]^T$	$[42114203 + 1.2, -30, 1.5]^T$	5000	0.5	50%
Case 4	$[42114203 - 0.3, 0, -0.2]^T$	$[42114203 + 1.2, -29.2, 1.5]^T$	20000	0.5	50%
Case 5	$[42114203 - 0.3, 0, -0.2]^T$	$[42114203 + 1.2, -29.2, 1.5]^T$	5000	0.5	25%, 99.99%
Case 6	$[42114203 - 0.3, 0, -0.2]^T$	$[42114203 + 1.2, -29.2, 1.5]^T$	5000	4, 0.1	50%

The attitude control torque for the ROGER spacecraft during deorbiting process is as follows:

$$\mathbf{T}_C = \left(K_P\varphi_A + K_D\dot{\varphi}_A\right)\mathbf{i}_A + \left(K_P\theta_A + K_D\dot{\theta}_A\right)\mathbf{j}_A + \left(K_P\psi_A + K_D\dot{\psi}_A\right)\mathbf{k}_A. \tag{21}$$

K_P and K_D are the proportional and differential coefficients.

5. Numerical Simulations

International System of Units is adopted except special statements. The initial roll, pitch, and yaw angles are 3/57.3, 4/57.3, and 5/57.3, respectively, and the corresponding Euler angular velocities are zeros. The tensor of moment of inertia of the ROGER spacecraft is as follows:

$$\mathbb{J}_A = \begin{bmatrix} 1000 & -49 & 32 \\ -49 & 1000 & 43 \\ 32 & 43 & 1000 \end{bmatrix}. \tag{22}$$

The initial orbital positions and velocities of the ROGER and abandoned spacecraft are denoted by $\mathbf{Rm}_0$, $\mathbf{Rs}_0$, $\mathbf{Vm}_0$, and $\mathbf{Vs}_0$, respectively. $\mathbf{Vm}_0$ and $\mathbf{Vs}_0$ are both selected as $[0, 3076.5, 0]^T$ in this paper. And the radius of the earth is 6378145, and the gravitational constant is $\mu = 3.9860044 \times 10^{14}$. The amplitude of the thrust is 20. The parameters mentioned above will be used throughout the paper.

The deorbiting results in Case 1 adopting the certain parameters will be regarded as the benchmark. In Case 2, $\mathbf{Rm}_0$ and $\mathbf{Rs}_0$ are changed to reduce the librations dramatically. The deorbiting results with comparatively large (Case 1) librations and few (Case 2) librations will be presented and compared.

In Case 3, $\mathbf{Rm}_0$ and $\mathbf{Rs}_0$ are changed to increase the initial tension force in the tether. The deorbiting results with smaller force (Case 1) larger force (Case 3) will be presented and compared.

In Case 4, k is selected as 20000 to see how the deorbiting results are affected by the elasticity of the tether. In Cases 5 and 6, η and T are selected as 25%, 99.99% and 4, 0.1 to see how the deorbiting results are affected by the two parameters.

The parameters in all cases can be found in Table 1.

The deorbiting results for Case 1 are presented in Figures 7–12.

The tensionless and tensional states are alternate during the deorbiting process by observing Figure 7; moreover,

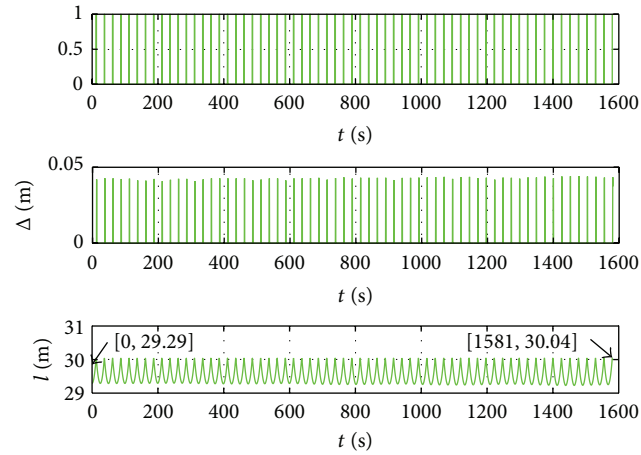

Figure 7: The tensional (1) and tensionless (0) states, the elongation of the tether (Δ), and the distance between two spacecraft (l) during deorbiting.

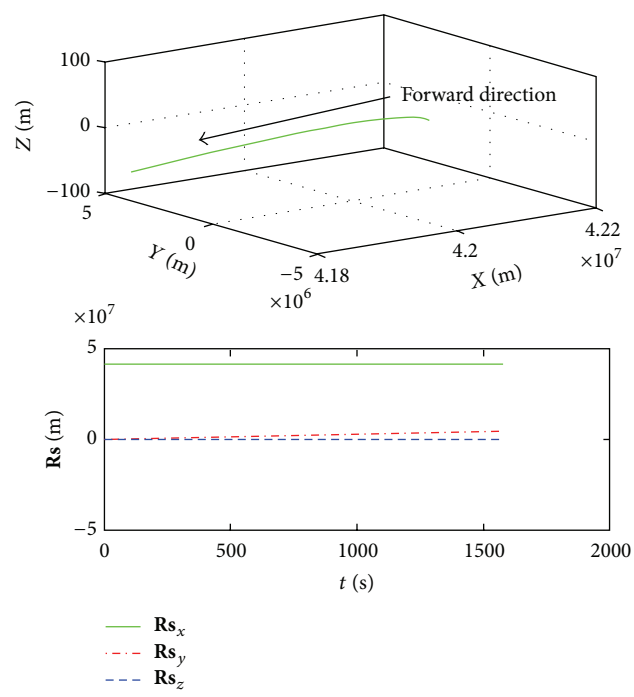

Figure 8: The trajectory of the abandoned spacecraft.

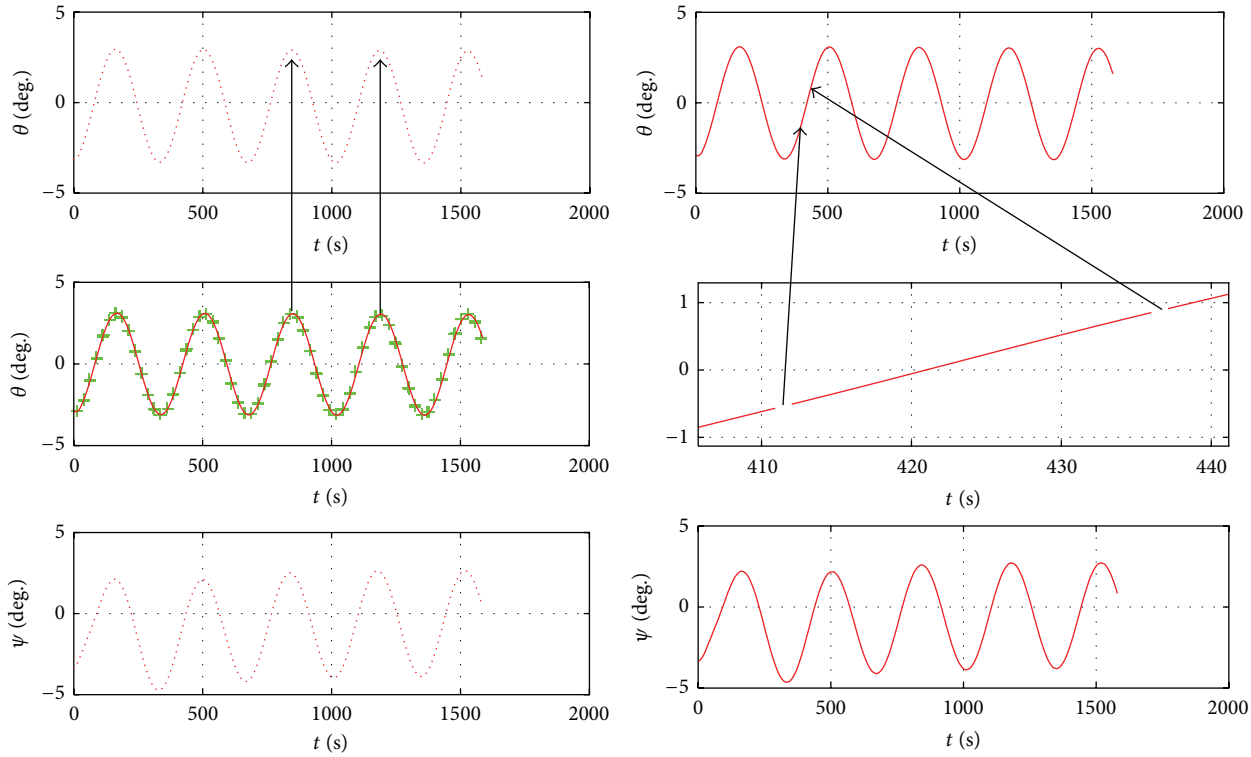

Figure 9: The equivalent expression of in-plane (θ) and out-plane (ψ) librations.

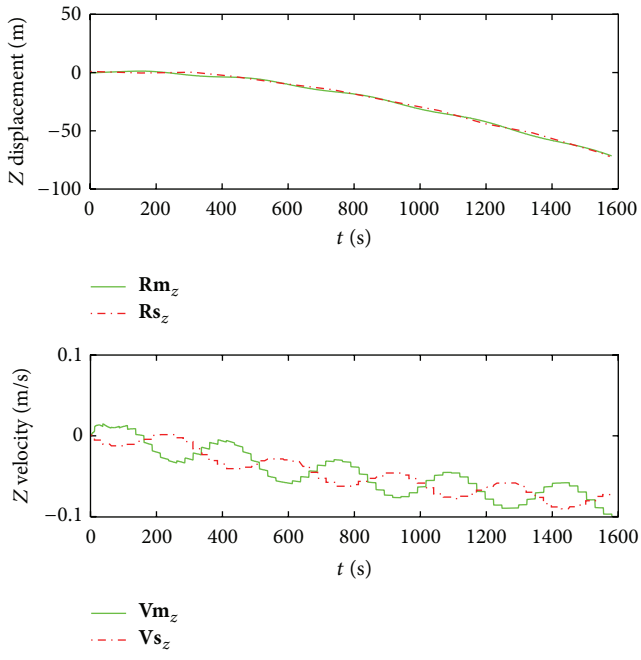

Figure 10: The out-plane positions and velocities of ROGER (m) and abandoned (s) spacecraft.

the tether is tensionless most of the time. And the distance is between 30 and 29 m; it can be seen that the deorbiting process is stable and the collision between the two spacecraft is avoided.

The 3D trajectory of the abandoned spacecraft is given in Figure 8. It is evident that the out-plane displacement of the abandoned spacecraft is negative during the deorbiting process.

The in-plane (θ) and out-plane (ψ) librations are presented in Figure 9 based on the orbital position coordinates of the ROGER and abandoned spacecraft. The librations corresponding to tensional and tensionless states are plotted by sparse dots and almost continuous curves, respectively. And it can be seen that the librations (or we call it the relative orientation relation of the two spacecraft) are stable and the tether is tensionless most of time.

The out-plane positions and velocities of the ROGER and abandoned spacecraft are given in Figure 10. The out-plane positions are negative during deorbiting and the out-plane motion is stable.

The components of the tension force and disturbing torques caused by the tether are given in Figure 11. The disturbing torques can be utilized as the control torques for the traditional tethered system.

The angular rate and angle errors during deorbiting are plotted in Figure 12. It can be seen that the attitude motion affected by the disturbance torques is stable. It is concluded that the deorbiting process is acceptable by analyzing Figures 7–12.

The deorbiting results for Case 2 are presented in Figures 13–15.

The tensional and tensionless states, the elongation, and the distance showed in Figure 13 are almost the same as in Figure 7. The distance during deorbiting is hardly affected by librations when adopting the same parameters and other initial conditions. But the attitude motion of the ROGER

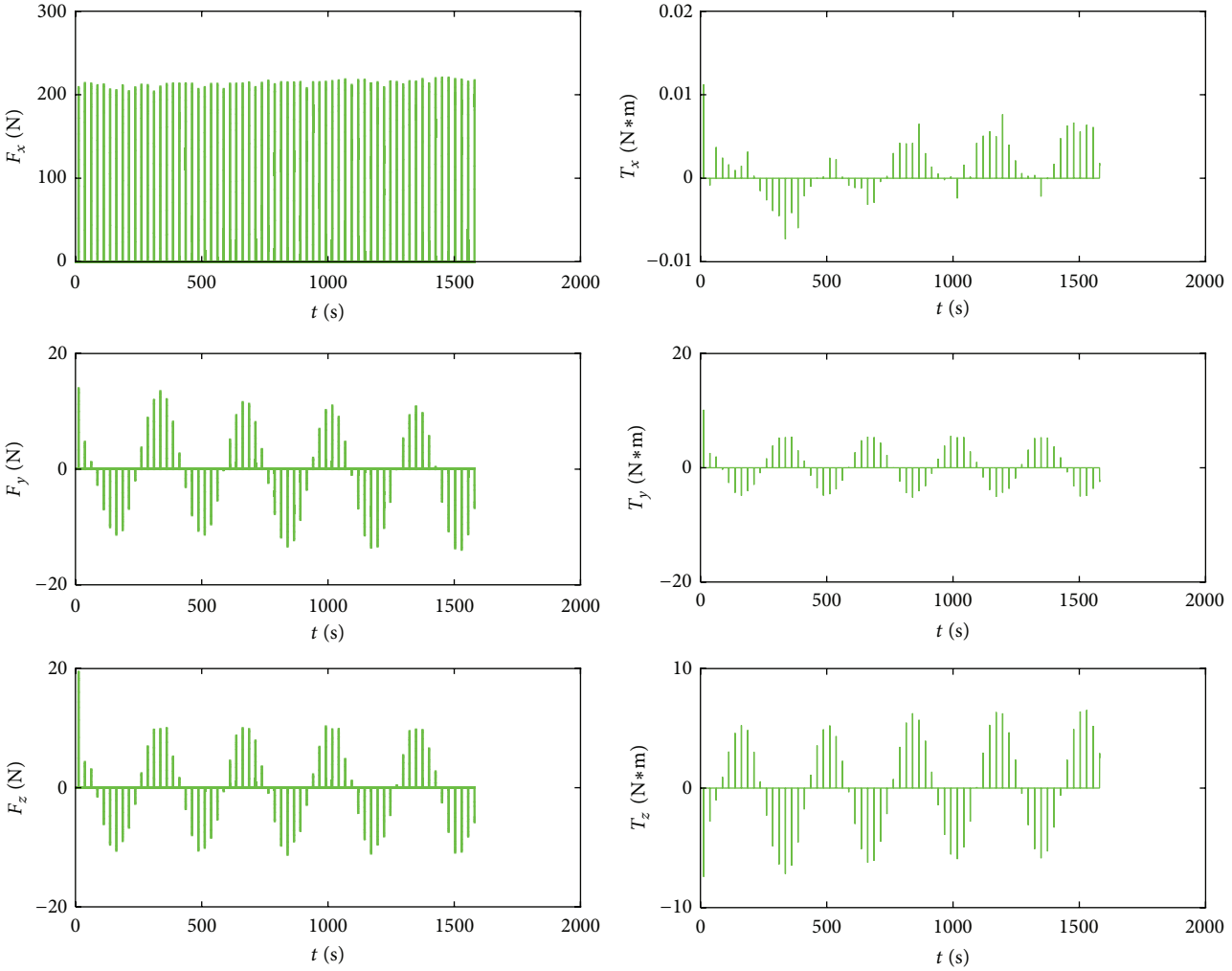

Figure 11: The components of the tension force (F_x, F_y, and F_z) and the disturbing torque (T_x, T_y, and T_z) in π_A caused by the tether.

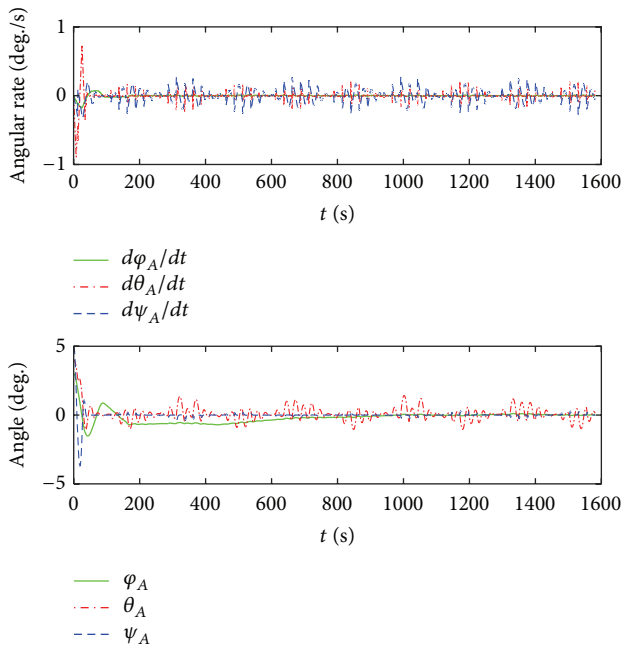

Figure 12: The angular rate and angle of the ROGER spacecraft.

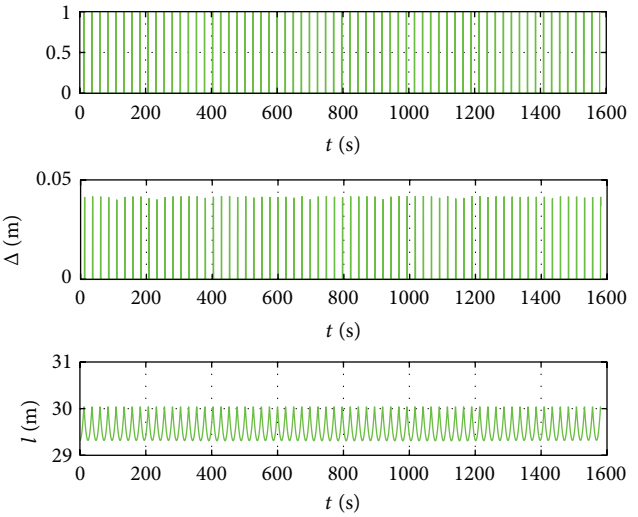

Figure 13: The tensional (1) and tensionless (0) states, the elongation of the tether (Δ), and the distance (l) between the two spacecraft.

spacecraft will be deeply affected by the librations by observing Figures 14-15.

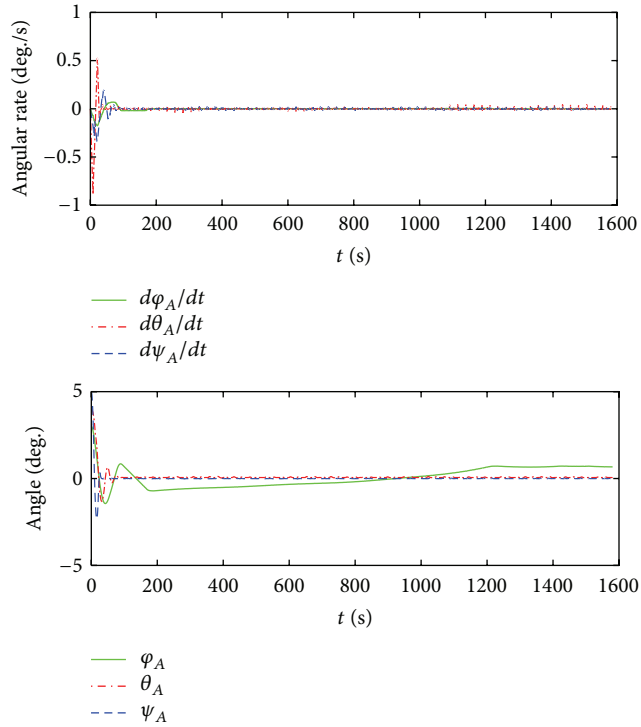

FIGURE 14: The angular rate and angle of the ROGER spacecraft.

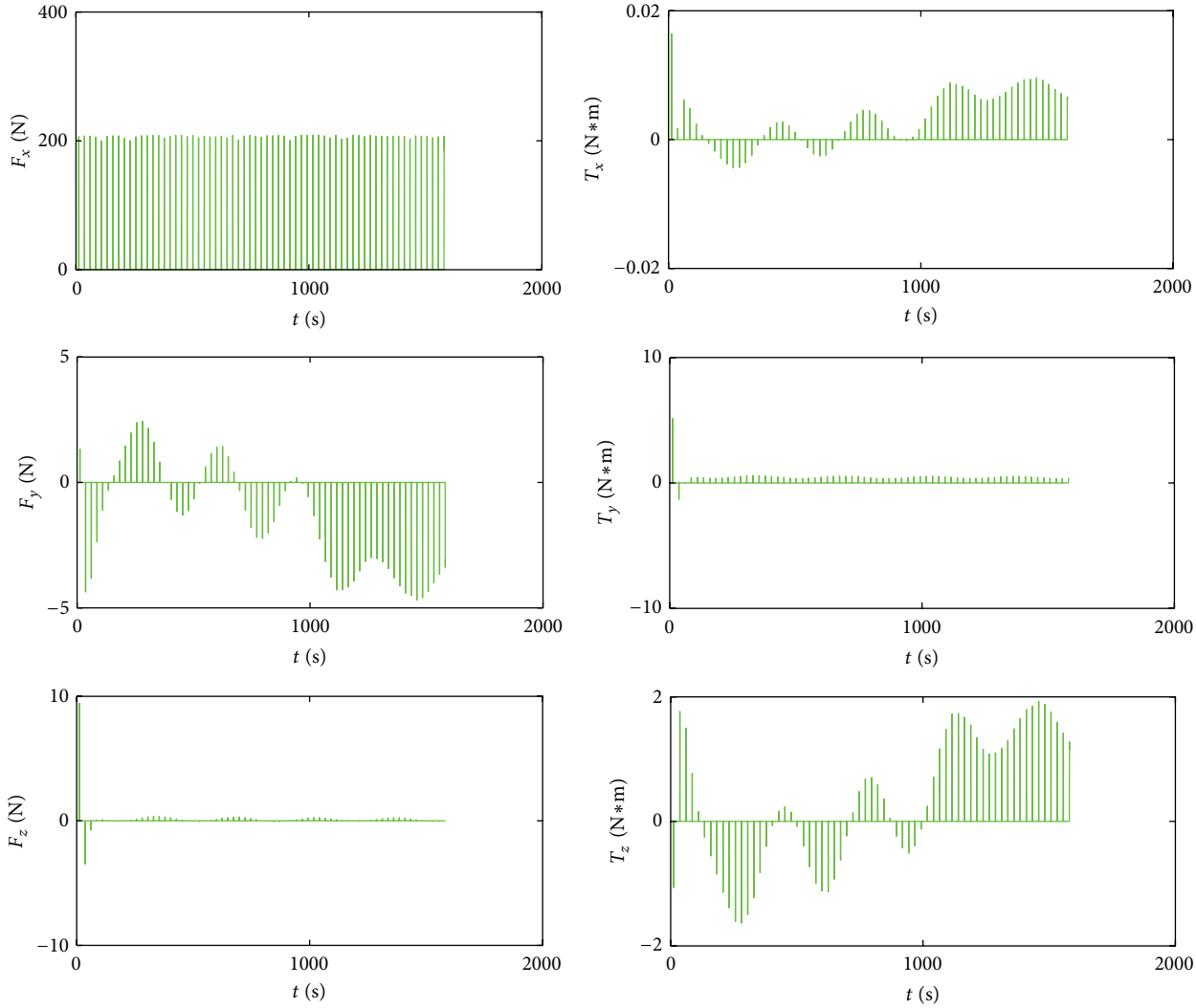

FIGURE 15: The components of the tension force (F_x, F_y, and F_z) and the disturbing torque (T_x, T_y, and T_z) in π_A caused by the tether.

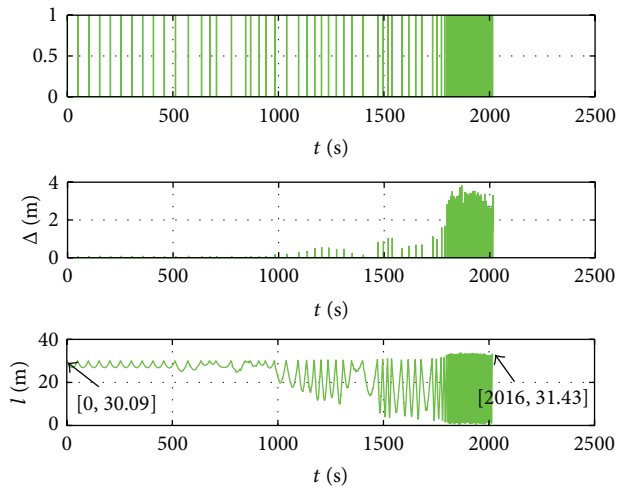

FIGURE 16: The tensional (1) and tensionless (0) states, the elongation of the tether (Δ), and the distance (l) between the two spacecraft.

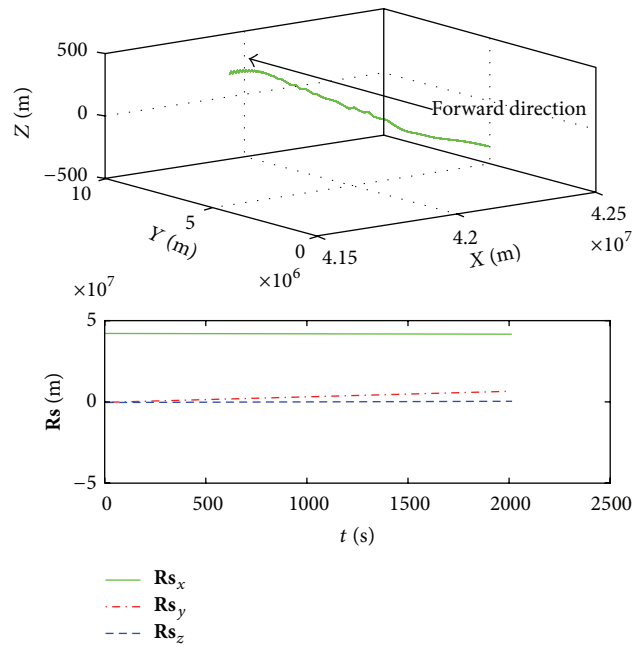

FIGURE 17: The deorbiting trajectory for abandoned spacecraft.

In order to study the attitude motion affected by the librations, the same control torque vector in Figure 12 is used to obtain the attitude motion in Figure 14. The attitude motions are more stable than the results in Figure 12 as the attitude motions are affected by the librations deeply. It also can be demonstrated by comparing the disturbing torques in Figure 11 with the torques in Figure 15. The larger the deorbiting system librates, the larger the disturbance torques will generate and the more unstable the system will be from the view of the ROGER spacecraft attitude motion.

The deorbiting results for Case 3 are presented in Figures 16–20.

It can be seen that the deorbiting results are very unsatisfactory in Figure 16 by comparing Figure 16 with Figure 7 as the initial tension force exists for the deorbiting process. The probability of collision sharply increases for this case. It is suggested that the initial tension should be small or zero.

It can be seen from Figure 17 that the out-plane orbital motion direction is along positive z-axis as observed in Figure 17.

The simulations in Figure 18 indicate that the librations are completely unstable and show bad behaviors. The maximum in-plane and out-plane angles both nearly reach 100 deg., respectively. This will be bad for deorbiting because of the great possibility of collision.

The time histories of the out-plane motions of the ROGER and abandoned spacecraft vary very sharply by observing Figure 19. Thus the deorbiting results under this condition are worse by comparing the results in Figure 10. The out-plane motions are unacceptable for a safe deorbiting.

The amplitude of the tension force is too large to assure the deorbiting process safety. The disturbing torques are so large that it is too difficult to control the attitude of ROGER spacecraft. Thus the parameters and initial conditions are completely unsuitable in this case.

The deorbiting results for Case 4 are presented in Figure 21.

It can be seen that the deorbiting results in Figure 21 are almost the same as in Figure 7. Thus it is concluded that the deorbiting results are hardly affected by the parameter "k."

The deorbiting results for Case 4 are presented in Figures 22-23.

The deorbiting results can be observed in Figure 22 under the condition of 99.99% duty cycle.

The deorbiting results can be observed in Figure 23 under the condition of 25% duty cycle.

It can be seen that the deorbiting results are bad when $\eta = 99.99\%$; on the contrary, the deorbiting process is good when $\eta = 25\%$. Thus it is concluded that η should not be that large in order to make the deorbiting safe.

The deorbiting results for Case 5 are presented in Figures 24-25.

The deorbiting results can be observed in Figure 24 under the condition of 4 s period.

The deorbiting results are as follows under the condition of 0.1 s period.

It can be concluded that deorbiting results are hardly affected by the period. But the extreme large period should not be adopted as the stability of the distance between the two spacecraft affected by the large period is studied deeply.

6. Conclusions and Future Work

The universal dynamic equations for ROGER system are derived during the entire deorbiting process. The simulation results and conclusions are obtained by adopting various parameters and initial conditions to study the deorbiting

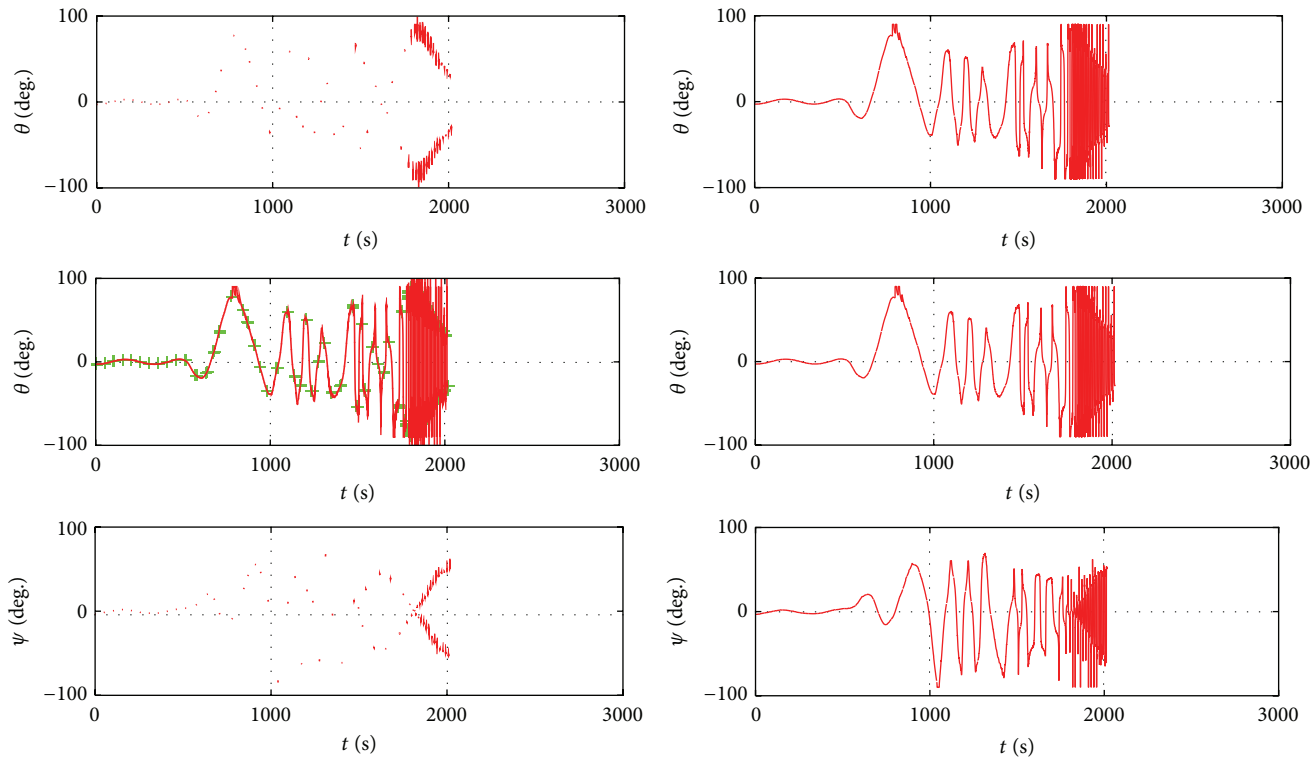

Figure 18: The equivalent expression of in-plane (θ) and out-plane (ψ) librations.

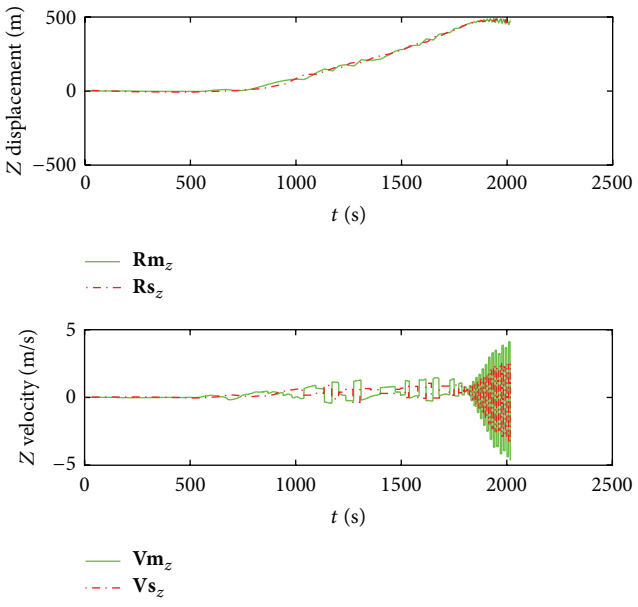

Figure 19: The out-plane positions and velocities of the ROGER (m) and abandoned (s) spacecraft.

results affected by these according parameters and initial conditions. The detailed conclusions are as follows:

(1) Two groups of dynamic equations are obtained according to the tensional and tensionless states of the tether, respectively. Moreover, the reasons the equations cannot be adopted in this paper are analyzed. A simple and practical dynamic modeling strategy for entire deorbiting process is proposed, and the librations are also equivalently expressed.

(2) Most of the time, the tether is tensionless. The deorbiting effects affected by initial librations, initial distance (initial tension force) between the two spacecraft, the coefficient of elasticity of the tether, the duty ratio, and period of the thrust are analyzed. It is concluded as follows:

(a) The distance between the two spacecraft is hardly affected by librations under the condition of the same initial distance and other parameters. However, the few librations do benefit for attitude motion of the ROGER spacecraft.

(b) The initial distance should be within a reasonable range. If the initial tension force is excessively large when the tether is tensional, then the deorbiting results are bad as the least distance during deorbiting is too small to avoid collision and the librations are nearly unstable; moreover, the attitude motion of the ROGER spacecraft is badly affected by this large initial tension force.

(c) The deorbiting process is hardly affected by the elasticity of the tether.

(d) The condition of 25% duty cycle is better than that of 99.99%; thus the more the duty cycle of the thrust force is, the worse the deorbiting results are.

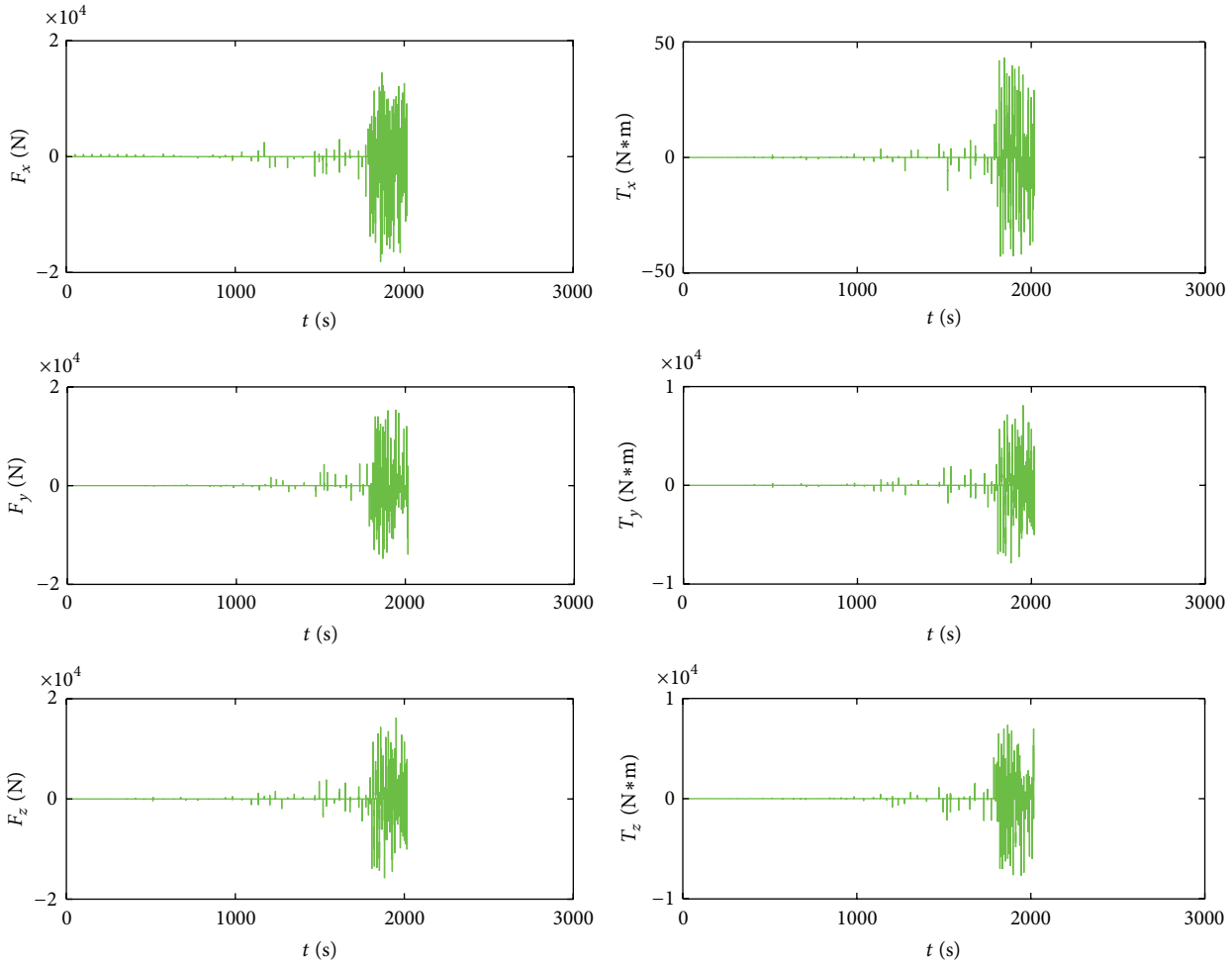

Figure 20: The components of the tension force (F_x, F_y, and F_z) and the disturbing torque (T_x, T_y, and T_z) in π_A caused by the tether.

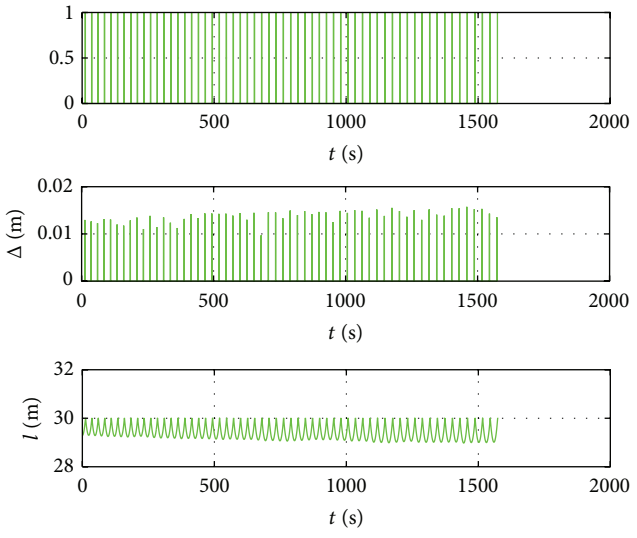

Figure 21: The tensional and tensionless states, the elongation of the tether, and the distance between the two spacecraft.

(e) The deorbiting results under the conditions of 4 s, 0.1 s, and 0.5 s period of the thrust force are almost the same; thus within a reasonable range of period, the deorbiting results are hardly affected by the period of the thrust force.

(3) It can be seen that the tether is tensionless most of the time; the tension force and the torques caused by librations and the tension force are so complex; thus the torques are difficult to be utilized as control torques in this paper.

(4) The librations equivalently expressed by the position vectors of the two spacecraft never exist singularity and thus show better advantages than the traditional definition.

The further studies are as follows:

(1) The more complex dynamic equations based on the modeling strategy in this paper considering the offset of the tether, the attitude, and orbital motions of the two spacecraft and the movable attachment between abandoned spacecraft and the tether should be established.

(2) More simulations should be carried out to study the deorbiting results affected by libations, distance

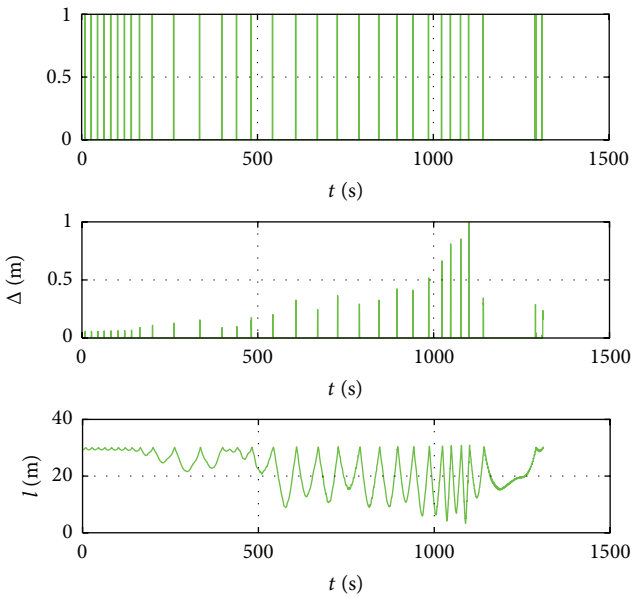

Figure 22: The tensional and tensionless states, the elongation of the tether, and the distance between the two spacecraft.

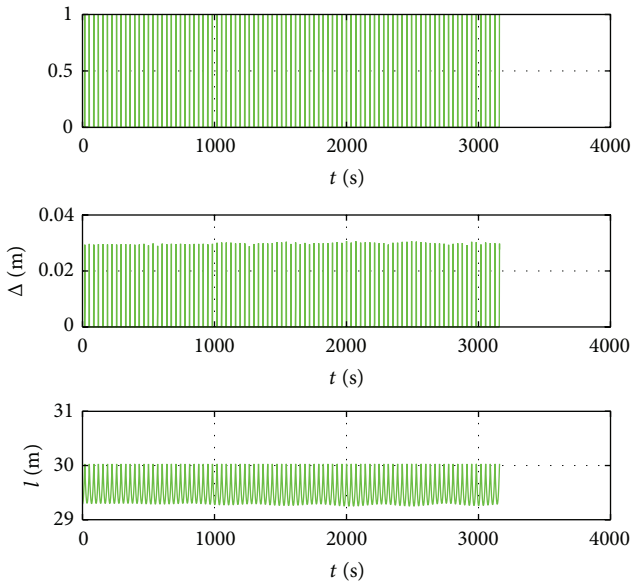

Figure 23: The tensional and tensionless states, the elongation of the tether, and the distance between the two spacecraft.

between the two spacecraft and the coefficient of elasticity of the tether, and so forth. Moreover, the superior deorbiting parameters and initial conditions should be summarized based on the simulations.

(3) The stability conditions for librations should be proved theoretically. The stability of librations under the conditions of small initial librations is merely speculated through simulations and will be hard to be assured if the initial libations are large.

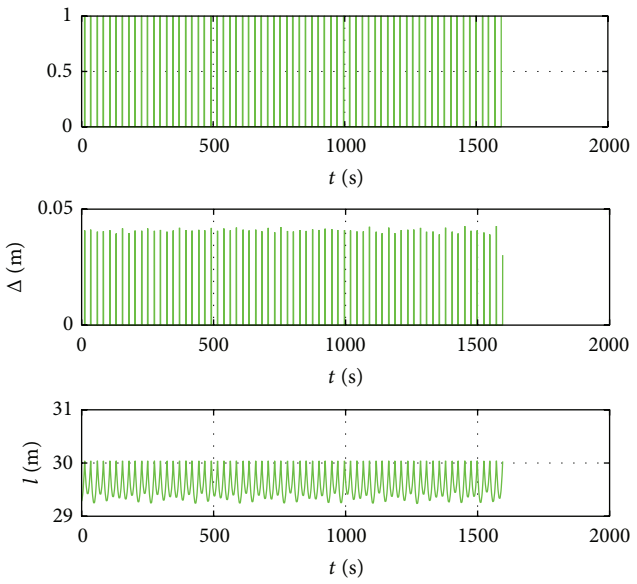

Figure 24: The tensional and tensionless states, the elongation of the tether, and the distance between the two spacecraft.

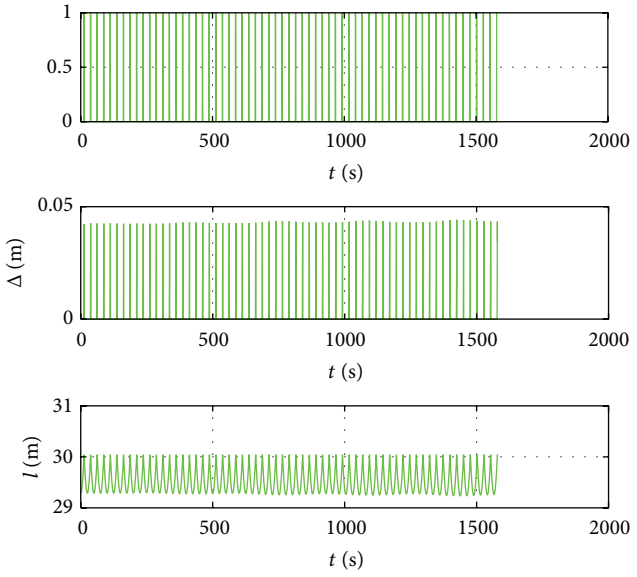

Figure 25: The tensional and tensionless states, the elongation of the tether, and the distance between the two spacecraft.

(4) How to utilize the torques caused by the offset and tension force of the tether as attitude control torques is worthy of being studied.

(5) The paper merely considers the dynamic modeling problems, and the optimal orbital transfer problems should be considered in detail.

Conflict of Interests

The authors declare that there is no conflict of interests regarding the publication of this paper.

Acknowledgments

This work was supported partially by the National Natural Science Foundation of China (Project nos. 11302134, 11272101). The authors highly appreciate the above financial support. The authors would like to thank the reviewers and the editor for their comments and constructive suggestions that helped to improve the paper significantly.

References

[1] W. Xu, B. Liang, B. Li, and Y. Xu, "A universal on-orbit servicing system used in the geostationary orbit," *Advances in Space Research*, vol. 48, no. 1, pp. 95–119, 2011.

[2] D. A. Smith, C. Martin, M. Kassebom et al., "A mission to preserve the geostationary region," *Advances in Space Research*, vol. 34, no. 5, pp. 1214–1218, 2004.

[3] F. Piergentili and F. Graziani, "SIRDARIA: a low-cost autonomous deorbiting system for microsatellites," Tech. Rep. IAC-06-B6.4.07, 2006.

[4] M. Kassebom, D. Koebel, C. Tobehn et al., "ROGER—an advanced solution for a geostationary service satellite," in *Proceedings of the 26th American Control Conference*, Chicago, Ill, USA, June 2000.

[5] B. Bischof, L. Kerstein, J. Starke et al., "Roger-robotic geostationary orbit restorer," in *Proceedings of the 54th International Astronautical Congress of the International Astronautical Federation (IAC '03)*, pp. 1365–1373, IAF, Bremen, Germany, September-October 2003.

[6] C. Pardini, T. Hanada, and P. H. Krisko, "Benefits and risks of using electrodynamic tethers to de-orbit spacecraft," *Acta Astronautica*, vol. 64, no. 5-6, pp. 571–588, 2009.

[7] C. Pardini, T. Hanada, P. H. Krisko, L. Anselmo, and H. Hirayama, "Are de-orbiting missions possible using electrodynamic tethers? Task review from the space debris perspective," *Acta Astronautica*, vol. 60, no. 10-11, pp. 916–929, 2007.

[8] V. Lappas, L. Visagie, N. Adeli, T. Theodorou, J. Ferndnez, and W. H. Steyn, "CubeSail: a low cost small cubesat mission for solar sailing and deorbiting LEO objects," in *Proceedings of the 2nd International Symposium on Solar Sailing (ISSS '10)*, New York, NY, USA, July 2010.

[9] C. Lucking, C. Colombo, and C. Mcinnes, "A passive high latitude deorbiting strategy," in *Proceedings of the 25th Annual IAA/USU Conference on Small Satellites*, Logan, Utah, USA, August 2011.

[10] G. Zhai, Y. Qiu, B. Liang, and C. Li, "System dynamics and feedforward control for tether-net space robot system," *International Journal of Advanced Robotic Systems*, vol. 6, no. 2, pp. 137–144, 2009.

[11] W. Xu, B. Liang, C. Li, Y. Liu, and X. Wang, "A modelling and simulation system of space robot for capturing non-cooperative target," *Mathematical and Computer Modelling of Dynamical Systems*, vol. 15, no. 4, pp. 371–393, 2009.

[12] J. A. Bonometti, K. F. Sorensen, J. W. Dankanich, and K. L. Frame, "Status of the momentum eXchange electrodynamic reboost (MXER) tether development," in *Proceedings of the 42nd AIAA/ASME/SAE/ASEE Joint Propulsion Conference & Exhibit*, Sacramento, Calif, USA, July 2006.

[13] G. Khazanov, A. L. Huntsville, E. Krivorutsky, and K. Sorensen, "Analyses of bare-tether systems as a thruster for MXER studies," in *Proceedings of the 41st AIAA/ASME/SAE/ASEE Joint Propulsion Conference and Exhibit*, Tucson, Ariz, USA, July 2005.

[14] Y. Ishige, S. Kawamoto, and S. Kibe, "Study on electrodynamic tether system for space debris removal," *Acta Astronautica*, vol. 55, no. 11, pp. 917–929, 2004.

[15] E. Kim and S. R. Vadali, "Modeling issues related to retrieval of flexible tethered satellite systems," *Journal of Guidance, Control, and Dynamics*, vol. 18, no. 5, pp. 1169–1176, 1995.

[16] S. Bergamaschi, F. Bonon, and M. Legnami, "Spectral analysis of tethered satellite system-mission 1 vibrations," *Journal of Guidance, Control, and Dynamics*, vol. 18, no. 3, pp. 618–624, 1995.

[17] S. Bergamaschi, P. Zanetti, and C. Zottarel, "Nonlinear vibrations in the tethered satellite system-mission 1," *Journal of Guidance, Control, and Dynamics*, vol. 19, no. 2, pp. 289–296, 1996.

[18] M. Pasca, M. Pignataro, and A. Luongot, "Three-dimensional vibrations of tethered satellite system," in *Proceedings of the 3rd International Conference on Tethers in Space-Toward Flight*, San Francisco, Calif, USA, May 1989.

[19] S. Pradhan, V. J. Modi, and A. K. Misra, "Simultaneous control of platform attitude and tether vibration using offset strategy," in *Proceedings of the AIAA/AAS Astrodynamics Conference*, San Diego, Calif, USA, July 1996.

[20] P. Williams, C. Blanksby, P. Trivailo, and H. A. Fujii, "Libration control of flexible tethers using electromagnetic forces and moveable attachment," in *Proceedings of the AIAA Guidance, Navigation, and Control Conference and Exhibit*, Austin, Tex, USA, August 2003.

[21] P. Williams, "Energy rate feedback for libration control of electrodynamic tethers," *Journal of Guidance, Control, and Dynamics*, vol. 29, no. 1, pp. 221–223, 2006.

[22] P. Williams, "Electrodynamic tethers under forced-current variations part 1: periodic solutions for tether librations," *Journal of Spacecraft and Rockets*, vol. 47, no. 2, pp. 308–319, 2010.

[23] P. Williams, "Electrodynamic tethers under forced-current variations. Part 2. Flexible-tether estimation and control," *Journal of Spacecraft and Rockets*, vol. 47, no. 2, pp. 320–333, 2010.

[24] M. Inarrea and J. Pelaez, "Libration control of electrodynamic tethers using the extended time-delayed autosynchronization method," *Journal of Guidance, Control, and Dynamics*, vol. 33, no. 3, pp. 923–933, 2010.

[25] H. Kojima and T. Sugimoto, "Stability analysis of in-plane and out-of-plane periodic motions of electrodynamic tether system in inclined elliptic orbit," *Acta Astronautica*, vol. 65, no. 3-4, pp. 477–488, 2009.

[26] H. Kojima and T. Sugimoto, "Stability analysis of periodic motion of electrodynamic tether system in elliptic orbit," in *Proceedings of the AIAA Guidance, Navigation and Control Conference and Exhibit*, Honolulu, Hawaii, USA, August 2008.

[27] S. Pradhan, V. J. Modi, and A. K. Misra, "Tether-platform coupled control," *Acta Astronautica*, vol. 44, no. 5-6, pp. 243–256, 1999.

[28] K. Kumar and K. D. Kumar, "Pitch and roll attitude maneuver of twin-satellite systems through short tethers," *Journal of Spacecraft and Rockets*, vol. 37, no. 2, pp. 287–290, 2000.

[29] K. D. Kumar and K. Kumar, "Satellite pitch and roll attitude maneuvers through very short tethers," *Acta Astronautica*, vol. 44, no. 5-6, pp. 257–265, 1999.

[30] S. Pradhan, V. J. Modi, and A. K. Misra, "On the offset control of flexible nonautonomous tethered two-body systems," *Acta Astronautica*, vol. 38, no. 10, pp. 783–801, 1996.

[31] R. E. Stevens and W. P. Baker, "Optimal control of a librating electrodynamic tether performing a multirevolution orbit change," *Journal of Guidance, Control, and Dynamics*, vol. 32, no. 5, pp. 1497–1507, 2009.

[32] E. L. M. Lanoix, A. K. Misra, V. J. Modi, and G. Tyc, "Effect of electrodynamic forces on the orbital dynamics of tethered satellites," *Journal of Guidance, Control, and Dynamics*, vol. 28, no. 6, pp. 1309–1315, 2005.

[33] P. Williams, "Optimal orbital transfer with electrodynamic tether," *Journal of Guidance, Control, and Dynamics*, vol. 28, no. 2, pp. 369–372, 2005.

[34] T. Watanabe, T. Makida, H. A. Fujii, H. Kojima, and W. Singhose, "An application of input shaping for electrodynamic tether system," in *Proceedings of the AIAA/AAS Astrodynamics Specialist Conference and Exhibit*, pp. 1442–1453, Providence, RI, USA, August 2004.

[35] H. J. Pernicka, M. Dancer, and A. Abrudan, "Simulation of the dynamics of a short tethered satellite system," in *Proceedings of the AIAA/AAS Astrodynamics Specialist Conference and Exhibit*, Providence, RI, USA, August 2004.

[36] J. Valverde, J. L. Escalona, J. Mayo, and J. Domínguez, "Dynamic analysis of a light structure in outer space: short electrodynamic tether," *Multibody System Dynamics*, vol. 10, no. 1, pp. 125–146, 2003.